

# Can cold pools lead to the development of low-level jets?

E. W. Luiz<sup>1\*</sup>, and S. Fiedler<sup>1,2</sup>

<sup>1</sup>Institute for Geophysics and Meteorology, University of Cologne, Cologne, Germany

<sup>2</sup>now: GEOMAR Helmholtz Centre for Ocean Research Kiel & Faculty for Mathematics and Natural Sciences, Christian-Albrechts-University Kiel, Germany

## Key Points:

- Observed low-level jets connected to cold pools were about 5% of all jet profiles during summer campaign in Germany.
- Cold pools favoured reduced frictional coupling of the wind field as a prerequisite for generating low-level jets during daytime.
- Low-level jets connected to cold pools were on average weaker but gustier than nocturnal jets.

---

\*Current address, Pohligstr. 3, 50969 Cologne, Germany

Corresponding author: Eduardo Weide Luiz, [eweidelu@uni-koeln.de](mailto:eweidelu@uni-koeln.de)

## Abstract

We present the first observational evidence for convectively generated cold pools (CP) as driving mechanism for low-level jets (LLJ). Our findings are based on a unique campaign dataset that allowed us to perform a systematic assessment of the process. During the three-month campaign in Germany, 4.7% of all identified LLJ profiles were connected to a CP (CPLLJ). Most measured CPLLJs appeared with the CP front and lasted for up to two hours. Moreover, we have observed a CP favouring the formation of a several-hours long LLJ. In that case, a strong LLJ and cooling of the atmosphere between the surface and at least 400 m a.g.l. were seen when the density current reached the measurement site. The development led to the formation of a near-surface temperature inversion during daytime as a prerequisite for the LLJ, not unlike the mechanism of nocturnal LLJs.

## Plain Language Summary

Low-level jets (LLJ) are strong winds that occur in the lowest few hundred meters of the atmosphere. Their influence ranges from transporting moisture and pollutants, to impacts on aviation safety and wind power production. LLJs typically occur at night, when the surface strongly cools, e.g., during cloud-free skies. Newly available measurement data from a campaign in summer 2021 gives us the unique opportunity to test the hypothesis that LLJs can also be driven by a cold pool (CP). CPs are areas of relatively cool and dense air formed by downdrafts underneath precipitating clouds. Our study provides the first observational evidence that CPs can favour the generation of a temperature inversion, with reduced friction of the winds with the surface, as a prerequisite for generating LLJs also during daytime. The observations show how CPs and LLJs are connected to each other.

## 1 Introduction

Low-level jets (LLJ) are wind speed maxima in the lowest 50–500 m of the troposphere (e.g., Shapiro & Fedorovich, 2010; Ziemann et al., 2020). They have implications for the transport of moisture and pollutants (e.g., Angevine et al., 2006; Chen & Tomassini, 2015), for aviation safety (e.g., Blackadar, 1957), the formation of dust storms (e.g., Schepanski et al., 2009), and wind power production (e.g., Gutierrez et al., 2016; Lampert et al., 2016). In the classical theoretical description of inertial oscillations, LLJs develop due to the decoupling of nocturnal winds from the surface friction by the formation of a near-surface temperature inversion (Blackadar, 1957; Van de Wiel et al., 2010). These conditions typically occur at night, particularly during cloud-free conditions that allow strong radiative cooling of the surface (Sisterson & Frenzen, 1978; Beyrich, 1994). LLJs formed by this mechanism are often called Nocturnal LLJs (NLLJ).

Other driving mechanisms for LLJs are known. A LLJ can form when a near-surface temperature inversion is formed by warm air advection over relatively cooler near-surface air. The associated tilt of isobaric surfaces leads to a thermal wind that under certain conditions can manifest itself as a LLJ. This mechanism can, for instance, play a role over gently sloping terrain and coastal areas, when a sufficiently large temperature gradient due to differential heating occurs (Mahrt et al., 2014; Kalverla, Duncan, et al., 2019; Svensson et al., 2019). Kilometre-scale regional model simulations, which partially resolve convective processes, further suggest that LLJs in summertime West Africa can be connected to convectively generated Cold Pools (CP) (Heinold et al., 2013), but due to the lack of suitable observational data, was to date difficult to verify. CPs are mesoscale areas of relatively cool and dense air formed through downdrafts associated with evaporation of hydrometeors underneath precipitating clouds (Kirsch, Hohenegger, Klocke, Senke, et al., 2022). According to Heinold et al. (2013), the LLJ profiles are generated by aged cold pools from deep convective clouds that glide up over a radiatively gener-

ated stable near-surface layer. Up to date there was no adequate observational data for a systematic assessment of CPs as driving mechanism for LLJs. We now have the opportunity to overcome the past observational limits by combining different measurements that were collected during a unique observational campaign in summer 2021 (Hohenegger et al., in review). Specifically, we use the new dataset to test the hypothesis that LLJs can be driven by CPs and that this is due to their cooling effect on the near-surface layer itself.

## 2 Data and Methods

### 2.1 FESSTVal Campaign

This study is based on data from the Field Experiment on Submesoscale Spatio-Temporal Variability (FESSTVal, Hohenegger et al., in review), organized by the Hans-Ertel-Centre for Weather Research in Germany. The primary goal of FESSTVal is measuring sub-mesoscale to mesoscale variability employing a measurement strategy to cover three main aspects: boundary layer patterns, cold pools and wind gusts. The FESSTVal campaign took place from June to August 2021 in the region of the Meteorological Observatory Lindenberg – Richard Assmann Observatory (MOL-RAO) of the German Weather Service (DWD). MOL-RAO is situated in a rural area of the federated state Brandenburg in Eastern Germany (EG). The campaign was special due to a dense network for near-surface measurements, with 80 low-cost and custom-designed APOLLO (Autonomous cold POoL LOgger) stations and 19 WXT weather stations (Kirsch, Hohenegger, Klocke, & Ament, 2022). These stations were circularly distributed with a maximum radius of 30 km from the centre where the three supersites were located. The regional network of many near-surface temperature and humidity sensors was ideal for the measurement of CPs.

At all supersites, Doppler wind LIDAR instruments were installed for vertically resolved wind measurements over heights of several hundred meters, which are needed for observing LLJs. The supersites were located in Lindenberg ( $EG_L$ , 52.21°N, 14.13°E), Falkenberg ( $EG_F$ , 52.16°N, 14.14°E), and Birkholz ( $EG_B$ , 52.20°N, 14.19°E), with a distance of about  $\sim 6$  km between each other. The flat area around  $EG_F$  and  $EG_B$  is agriculturally used, with the latter having trees in the vicinity.  $EG_L$  is located in a more complex area with buildings and a hill. The LIDAR in  $EG_F$  and  $EG_B$  operated in the gust mode, i.e., a measurement configuration that allows wind measurements with  $\sim 3$  seconds temporal resolution (Steinheuer et al., 2022). The same gust mode was operated in  $EG_L$ , except for 01-10 June 2021 when the velocity azimuth display (VAD) method was used (Päschke et al., 2015). We compute 10 minute averages of the winds retrieved from the LIDAR measurements unless otherwise stated. Our analysis is based on data for all days that had at least 50% data coverage with the LIDAR. Taken together, we had sufficient LIDAR measurements on 72, 60 and 63 days in  $EG_F$ ,  $EG_L$  and  $EG_B$ .

We further used data for temporally continuous temperature profiling from a microwave radiometer (Löhnert et al., 2022) and tower measurements from 10-98 m in  $EG_F$ , and profiles from radiosondes (Kirsch, Stiehle, et al., 2022) in  $EG_L$ . Radiosondes were launched every six hours beginning at midnight as part of the standard measurement of MOL-RAO. Additional soundings were carried out at times in between the standard times when events of special interest occurred. For the analysis of the atmospheric stratification, we calculated virtual potential temperature profiles and the Richardson Number ( $Ri$ ) underneath the core of LLJs from radiosondes in  $EG_L$  and from standard instruments for weather monitoring that are mounted on a 100m high meteorological tower in  $EG_F$ . Large  $Ri$  values ( $Ri > 0.25$ ) imply that the stratification is stronger than shear-driven mixing. Unstable conditions and turbulent mixing are associated with negative  $Ri$  values (Han et al., 2021).

## 2.2 Automated Identifications

### 2.2.1 LLJ

We adopt an automated detection algorithm for LLJs for a systematic analysis of the data. Several approaches for LLJs exist, e.g., using relative (Banta et al., 2002; Tuononen et al., 2017; Wagner et al., 2019) or absolute (Andreas et al., 2000; Banta et al., 2002; Hallgren et al., 2020) criteria to identify sufficiently strong maxima in wind speed profiles. We adopt the method as in Luiz and Fiedler (2022) for the comparability of the results. The algorithm uses a vertical shear in the wind speed stronger than  $-0.005 \text{ s}^{-1}$  above the jet core for the characteristic nose of LLJs, paired with a minimum difference of  $2 \text{ ms}^{-1}$  between the jet core and the next minimum in the wind speed in the 500 m deep layer above the jet core. The jet core was defined as the first maximum in the wind speed in the lowest 500 m a.g.l..

Prior to the application of the LLJ detection algorithm, we smoothed the vertical profiles using moving averages every 5 measurement heights and obtained wind profiles with a vertical resolution of 26.5 m. The smoothing reduces the small scale and fast variability in the winds associated with turbulence. We then removed all detected LLJs shorter than 20 minutes since visual inspection showed that these were daytime profiles with strong turbulent changes in the wind speed with height. LLJs were detected in all vertical profiles for which we had at least 75% of data between the surface and 1000 m a.g.l.. We connected individual LLJ detections that are consecutive or have up to 20-minute gaps in between individual LLJs into one LLJ event. We therefore account for short intermittent mixing events during LLJs in the statistics.

### 2.2.2 Cold Pool

Past studies identified Cold Pools (CP) using different data ranging from boundary layer towers (Goff, 1976; Kirsch et al., 2021), moving instruments aboard aircrafts and ships (Terai & Wood, 2013; de Szoeke et al., 2017), precipitation radars (Borque et al., 2020), model data (Heinold et al., 2013) and a combination of instruments (Mueller & Carbone, 1987; Feng et al., 2015). In our study, we adapted the method from Kirsch et al. (2021) using 10 m temperature data from the measurement tower in *EG<sub>F</sub>*. The method defines a CP when a minimum temperature reduction by 2 K in a 20 minute time window is measured. The first 10 minutes with a temperature difference by 0.5 K is defined as the front of the CP. The subsequent temperature decrease during the next hour is identified as part of the same CP event. The results from this method were validated against a list of CP events from FESSTVaL based on a more complex and multi-site identification method using the sensor network (Kirsch, 2022). Compared to the FESSTVaL list, three CPs were not identified by our automated method, because of the lack of a sufficient temperature decrease in *EG<sub>F</sub>*. We did not identify a LLJ for these cases. There were also four CPs that were missed by the algorithm due to a too weak temperature reduction in *EG<sub>F</sub>*, but had a LLJ signature. We therefore manually added these four CPs to our statistics. All LLJs that fall onto the same time as a CP were classified as CPLLJ\*. All profiles from a LLJ event temporally connected to a CP, but not necessarily co-occurring with the CP, were classified as CPLLJ, i.e., all CPLLJ\* are included in the CPLLJ statistics.

## 3 Results

### 3.1 Statistics of LLJs

All supersites showed a similar frequency of occurrence for LLJs, with 20-23% of all available profiles. When accounting only for nocturnal profiles, adopting a solar height below  $20^\circ$ , the LLJ frequency increased to 32-34% of all profiles. The larger frequency

of LLJs during the night period indicates a higher probability for forming a nocturnal LLJ (NLLJ) along with a stably stratified surface layer following the concept of an inertial oscillation (e.g., Blackadar, 1957). To assess such NLLJs in more detail, we take all LLJs longer than six hours at nighttime. From these NLLJ profiles in  $EG_F$ , 74% coincided with the occurrence of near-surface temperature inversions, measured by an average increase of the air temperature with height in the first 200 m a.g.l.. The average  $Ri$  value between the surface and the NLLJ core at 00 UTC during NLLJs was 340. Both the temperature inversion and the strongly positive  $Ri$  are clear indicators of the reduced frictional effects on the winds in the NLLJ.

The co-occurrence of LLJs across the supersites depends on their duration. When a LLJs in  $EG_F$  occurred, we observed also a LLJ at the other two supersites in 75% of the cases. Restricting the analysis to events longer than 3 hours increased the LLJ co-occurrence to 84%. This is consistent with the perception that long-lived LLJs simultaneously occur over a larger spatial extent for similar atmospheric conditions. Differently, when analyzing events shorter than 3 hours, the co-occurrence decreased to 47%. This is to be expected since short LLJs can be associated with density currents from convective cold pools that may not affect all sites simultaneously or can be nocturnal LLJs perturbed by local conditions leading to intermittent vertical mixing at different times. Take for instance the measurements at  $EG_F$ . There, 92% of the days had at least one LLJ detection, but events longer than one (three) hour were detected in 68% (40%) of the days.

## 3.2 LLJs associated with cold pools

### 3.2.1 Statistical assessment

The results of the joint detection of CPs and LLJs highlight that 6.8% of all LLJ profiles in  $EG_F$  were directly connected to a CP (CPLLJ). LLJs at the same time as the passage of the CP (CPLLJ\*) add up to a fraction of 1.7% of the total number of LLJ profiles. From all CPLLJ profiles in  $EG_F$ , we have seen in about 27% of the cases a simultaneous occurrence of a LLJ at the other two supersites. The average length of CPLLJs was about two hours. CPLLJs in a triangular area with a side length of about six kilometers are therefore much shorter than NLLJs owing to the fact that the area with CPLLJ migrates in space over time and they have relatively short-lived driving mechanism. Down-drafts from deep convective clouds in the mid-latitudes generate the CPs. They are horizontally spreading density currents that are more local and short-lived for instance compared to the radiative cooling, that plays a continuous role in the nocturnal boundary layer across space as key process for NLLJs.

CPLLJs occur under substantially different synoptic-scale conditions than NLLJs. The wind rose in Figure 1a shows that winds in the core of CPLLJs had two prevailing directions around Northwest and East, with easterlies being overall dominant. These directions are very different compared to the statistics for NLLJs that have primarily South-easterlies in the core. These results point to the overall different meteorological conditions under which NLLJs and CPLLJs occur. For example, while NLLJs are favoured by anticyclonic weather patterns in Germany (Emeis, 2014; Luiz & Fiedler, 2022), our visual inspection of the weather charts for the identified CPLLJs pointed to the influence of a low pressure system (not shown). This result is consistent with the requirement of having a convective situation that allows for sufficient lift for the development of deep moist convection as origin of cold pools and CPLLJs.

CPLLJ were on average slightly weaker and lower than NLLJs. Figure 1b–c shows the distribution of the wind speed and the height of the jet cores. The mean wind speed in the core of CPLLJ (CPLLJ\*) was  $7.1$  ( $7.4$ )  $\text{ms}^{-1}$  at a mean height of 207 (190) m. This is about  $1.5 \text{ ms}^{-1}$  less compared to the average wind speed in the core of NLLJs ( $8.6 \text{ ms}^{-1}$ ) and at a lower height by about 20 m (227 m). At the same time, the wind gusts in the

core of CPLLJs were stronger, with speeds up to  $17.5 \text{ ms}^{-1}$  in  $EG_F$  exceeding the maximum of  $15 \text{ ms}^{-1}$  for NLLJs by  $2.5 \text{ ms}^{-1}$ . Closer to the surface, the differences in the winds were even larger than in the core. When we use the 40m-wind speeds as an example, we find that the winds during CPLLJs were on average weaker, but associated with stronger gusts compared to NLLJs (Figure 1d–e). The 10-minute averaged differences between the maximum 3s gust and the minimum 3s wind speed were for instance  $2.9 (1.9) \text{ ms}^{-1}$  during CPLLJs (NLLJs) at 40 m a.g.l. (Figure 1f) indicative for the sharp wind increases of CPLLJs that lead to wind-power ramps.

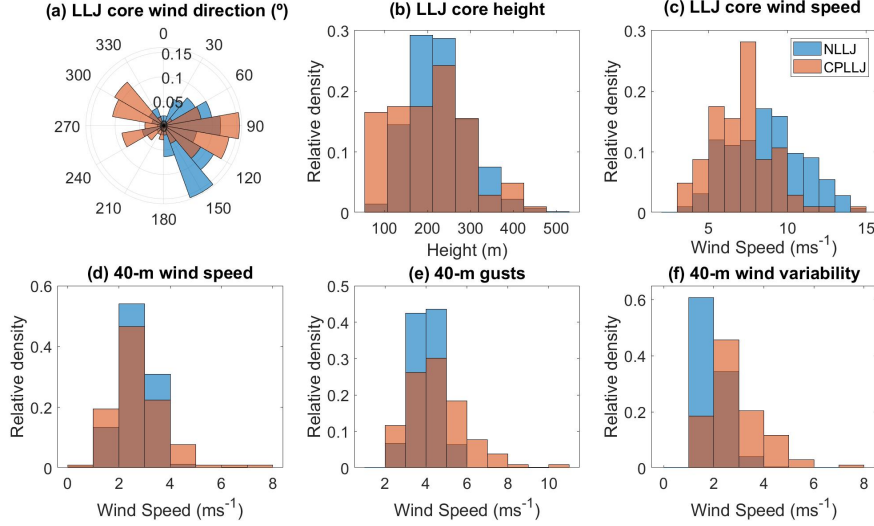


**Figure 1.** Relative density histograms of the wind during NLLJs and CPLLJs in  $EG_F$ . Shown are: (a) LLJ core wind direction, (b) LLJ core height, (c) LLJ core 10-min averaged wind speed, (d) 10-minutes averaged wind speed at 40 m, (e) 40 m wind gusts and (f) 40 m wind speed variability. Wind gusts are defined as the maximum 3s wind speed in 10-minutes intervals. The variability in (f) was calculated as the difference between the gust and the minimum wind speeds in the same 10-minutes intervals.

### 3.2.2 Temporal development

Most CPLLJ appeared together with the CP front and were seen in our measurements for up to two hours after the front had passed. However, we observed three CPLLJ events longer than two hours with one such case during the afternoon of 29 June 2021. This CPLLJ event lasted for about six hours at  $EG_F$  and was recorded at all supersites (Figure 2). The CP reached  $EG_F$  around 14 UTC (16 LT), leading to jet-like profiles at all three supersites and strong winds with 10-min averages of up to  $14 \text{ ms}^{-1}$ . At  $EG_F$ , the CPLLJ started at the same time when the CP front arrived. The winds in the CPLLJ core were strong, e.g., with gusts in the jet core (at 40 m) of up to  $21 (13) \text{ ms}^{-1}$  in  $EG_B$ . The CPLLJ persisted until about 19 UTC (21 LT) at  $EG_L$  and  $EG_F$ . In  $EG_B$ , the density current started slightly earlier due to the geographical position of the site upwind from the other two sites. There, the CPLLJ development was interrupted by a break of about one hour after the CP had passed. This difference is due to local influences on the winds since the other two sites had a continuous detection of a CPLLJ over time. We also see changing heights for the core of the CPLLJ, particularly in the first hour after the CP passage. This behaviour is possibly connected to a gravity wave in the wake of the migrating cold pool, e.g., known from other density currents (Udina et al., 2013). At  $EG_L$ , there was also a weak LLJ signature up to about 40 minutes ahead of the CP, pos-

sibly connected to upslope winds at the hill due to the strong daytime heating, reflected by a 2 m air temperature of 28°C before the arrival of the CP.

A CP can favour the formation of a surface-temperature inversion that results in a LLJ formation similar to NLLJs. We illustrate this mechanism with temperature and wind speed profiles. The CP arrived in  $EG_F$  around 14 UTC on 29 June 2021, visible as rapid reduction in the 10 m air temperature by 5.7°C within 20 minutes (Figure 2a and 3a). At the same time when the density current reached the site, a CPLLJ\* profile occurred. The CPLLJ\* shows the strongest wind speeds around 100 m a.g.l. with gusts of up to 17 ms<sup>-1</sup> at  $EG_F$ . The vertical profile of the wind speed has already the characteristic nose-like shape for a LLJ at all three sites when the CP front arrives (Figure 2b). At that time the temperature profile is, however, still indicating unstable stratification (Figure 3a and c). Ten minutes after the passage of the leading edge of the CP, a temperature inversion is first seen, the winds slacken throughout the profile and CPLLJs profiles are identified (Figure 2). Because this development begins in the daytime convective boundary layer (16 LT), it is a clear indicator that CPs can contribute to building a surface temperature inversion. In the case assessed here, the CP initially cooled all layers between the surface and up to at least 400 m a.g.l., leading to a stronger cooling of the layers closest to the surface behind the passage of the leading edge of the CP (Figure 3a). Ten minutes later, the levels below 200 m a.g.l. continued to cool, forming a temperature inversion as one would typically expect much later in the transition to night.

The formation of the temperature inversion reduced the frictional coupling of the winds in some distance to the surface in the wake of the CP, allowing LLJs to form already during the day with a mechanism similar to NLLJs. That change in stratification is seen ten minutes after the CP front, e.g., as inversion in the air temperature over the lowest 200 m in  $EG_F$  (Figure 2a). The newly formed CPLLJ in  $EG_F$  is continuously seen in the measurements until 19 UTC. During the CPLLJ lifetime, several intermittent mixing events occur indicated by the change in the vertical stratification and below-threshold  $Ri$ , particularly in the evening transition between 16 and 18 UTC, i.e., two to four hours after the CP front. After 18 UTC, the nocturnal radiative cooling sufficiently strengthens the surface inversion again to increase  $Ri$ . The development of low-level stratification including the height of the CPLLJs is clearly seen in the vertical profiles for virtual potential temperature from radiosondes in  $EG_L$  (Figure 3c-d). One hour ahead of the CP, the boundary layer has the typical daytime profile with unstable conditions close to the surface and a neutral stratification in the well-mixed layer with light winds throughout the boundary layer (13 UTC, 15 LT). At the time of the CP arrival in  $EG_L$  and  $EG_F$  (14 UTC, 16 LT), the virtual potential temperature decreased with height, indicative for convective mixing and a strong LLJ appears, with 14 ms<sup>-1</sup> in the core around 260 m a.g.l.. The virtual potential temperature profile shows a stably stratified surface layer in the wake of the CP (16 UTC, 18 LT) with a strong inversion between the surface up to 250 m a.g.l.. At that time, a CPLLJ was seen with a core around 500 m a.g.l. near the top of the surface inversion, in agreement with the LIDAR measurements. The  $Ri$  values support these findings with  $Ri=-259$  and  $Ri=-50$  at 13 and 14 UTC indicative for vertical mixing, and  $Ri=2950$  at 16 UTC that is characteristic for a stable stratification. The CPLLJ ended around 19 UTC (21 LT), thus around the time when NLLJ development would typically begin. In fact, NLLJs were mostly detected after 19 UTC during FES-STVaL. We suspect that the CPLLJ could have continued in the course of the night if no perturbation would have occurred. Although some periods of atmospheric stability were identified in the night after the CP event, the influence of a low pressure system prevent a sufficient reduction of the frictional coupling to the surface that would be needed for a NLLJ.

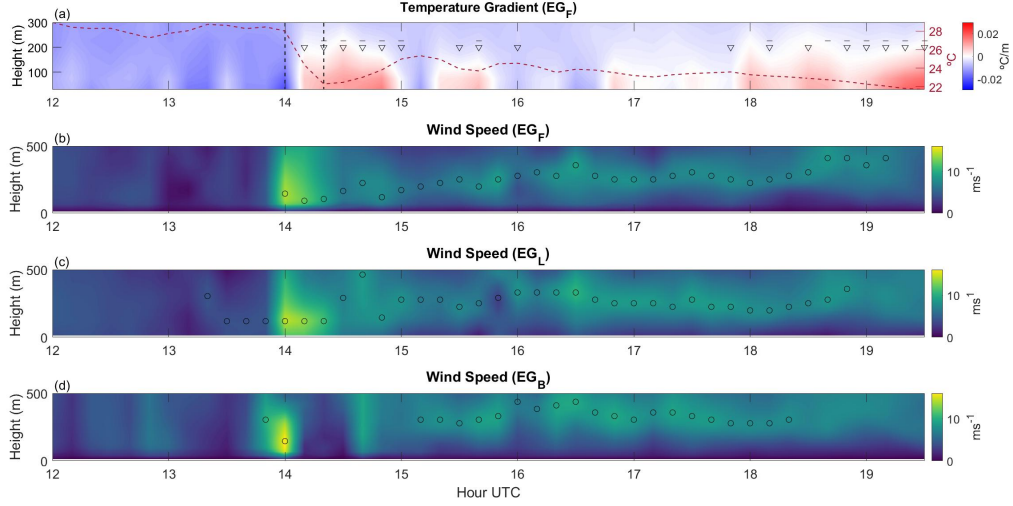


**Figure 2.** Temperature, stability metrics, and winds for the CPLLJ of 29 June 2021. Shown are time series (a) for (shading) the vertical gradient in air temperature from the microwave radiometer and (dashed line) the 10 m air temperature in  $EG_F$ , and (b–d) the (shading) vertical profiles of wind speeds in  $EG_F$ ,  $EG_L$  and  $EG_B$ . In a,  $\nabla$  and  $-$  mark the times with above-threshold  $Ri$  and positive vertical gradients in the virtual potential temperature calculated from the meteorological tower between 10 and 80 m as indicators for near-surface stable conditions, and the vertical dashed lines mark the start and end point of the automated CP detection. In b–d, black circles mark the automated detection of LLJs.

## 4 Discussion and Conclusion

The present study shows the first systematic assessment of convectively generated cold pools (CP) as driving mechanism for low-level jets (LLJ) based on new observations in Central Europe. We provide observational evidence for how a CP contributes to the formation of a surface-temperature inversion that allows a LLJ to develop in the wake of a CP. The connection of LLJs and CP events was earlier only documented in convection-permitting simulations over Africa (Heinold et al., 2013), describing dust storms simultaneously connected to LLJs and CPs. Heinold et al. (2013) inferred that aged cold pools glide up over a radiatively formed stable surface layer, triggering LLJ formation over a large area due to the locally induced pressure gradient. Our observational results highlight that a cold pool itself can help to form the surface inversion needed for a prolonged LLJ development. In the observed case, the boundary layer initially cooled the atmosphere up to at least 400 m a.g.l. when the CP arrived. The temperature inversion developed behind the leading edge of the CP, when the air below 200 m a.g.l. continued to cool. Since this development occurred during daytime when radiative cooling does not dominate the temperature development, it points to CPs as trigger for the formation of a surface inversion. The associated reduced frictional coupling of the wind with the surface allowed the generation of LLJs in the wake of the CP already during daytime and not unlike the mechanism of nocturnal LLJs. We did not observe a continuous turning of the wind for LLJs connected to cold pools (CPLLJ), but this is also not the case for most nocturnal LLJs at the site due to non-stationary conditions. The strongest near-surface temperature inversion is seen at the beginning of CPLLJ, namely up to one hour after the CP front. Due to the later weaker stability, the winds in the CPLLJ core were weaker and there was more vertical mixing than earlier during the event.

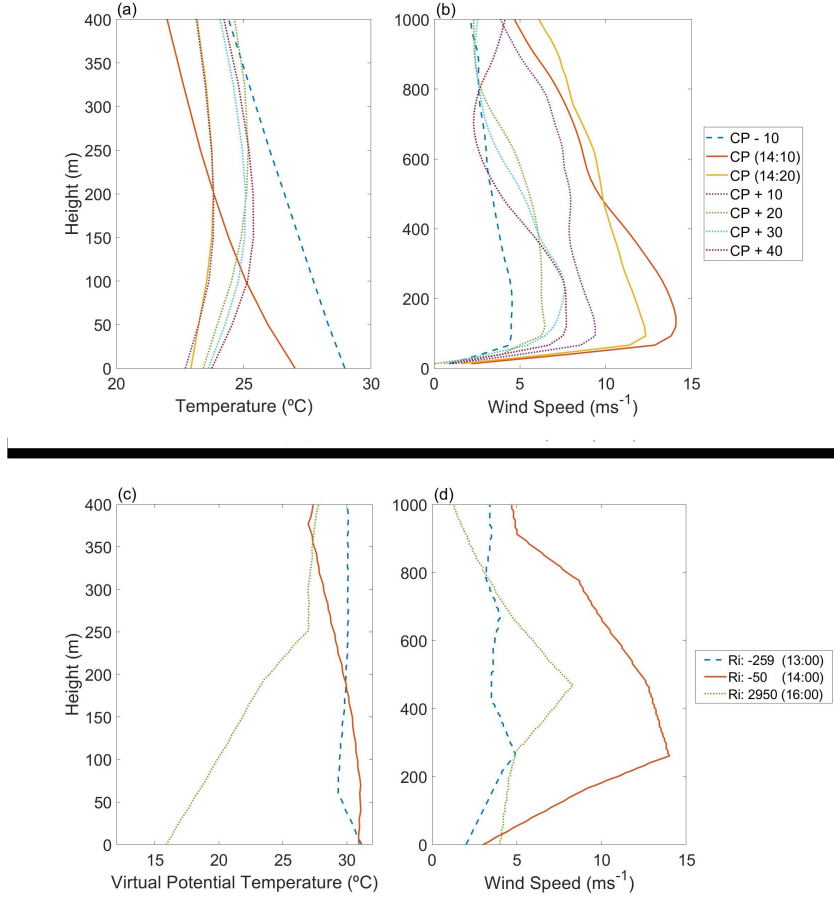


**Figure 3.** Vertical profiles during the CPLLJ of 29 June 2021 in Falkenberg at the top and Lindenberg at the bottom. Shown are vertical profiles of (a–b) temperature from the microwave radiometer and wind speed from the Doppler wind LIDAR in  $EG_F$ , (c–d) virtual potential temperature with the vertically averaged  $Ri$  and wind speed from the radiosondes in  $EG_L$ . CP in a,b are the 10-min averaged profiles at the time of the automatically identified CP, with  $\pm$  indicating the time difference relative to the CP in minutes. All times are in UTC.

LLJs connected to cold pools (CPLLJ) comprised 4.7% of the LLJ profiles in summer 2021. The average lifetime of CPLLJs was two hours. Due to their low frequency of occurrence, CPLLJs do not strongly influence LLJ climatologies in regions where convective downdrafts play a minor role, but some of their characteristics, e.g. stronger gusts and wind variability compared to nocturnal LLJs, can have adverse impacts, e.g., for wind power production (Kalverla, Duncan Jr, et al., 2019) which becomes increasingly important as Europe moves towards more wind power capacities to reach climate-neutrality. The lower height and gusty winds associated with CPLLJs have for instance impacts on wind turbines and the operation of wind parks feeding electricity into the transmission grid that needs to keep a stable frequency within a tight range to avoid blackouts. Rapid temporal changes in wind speeds like during CPLLJs can lead to strong power fluctuations also known as power ramps. These can be technically balanced, but need to be known early enough, e.g., from forecasts and from climatological assessments. To that end, we compared the observed CPLLJs against ERA5 reanalysis data and found that none of the CPLLJs were simulated by the model (not shown). It indicates that a driv-

ing mechanism of LLJs is entirely missing. There is good reason to believe that this might also be true for other weather and climate models with parameterized convection, e.g., indicated by the challenge to simulate cloud processes (Bony et al., 2015). Although CPLLJ are rare in Germany, they can be much larger and more frequent elsewhere, e.g., indicated by storm-resolving simulations in the Saharan desert (Heinold et al., 2013). Future research might advance our understanding of CPLLJ statistics, when more storm-resolving simulations become available.

## Open Research

All FESSTVaL data is available in the SAMD archive found at <https://www.cen.uni-hamburg.de/en/icdc/data/atmosphere/samd-st-datasets/samd-st-fesstval.html>. The LIDAR data using gust mode can be found at <https://doi.org/10.25592/uhhfdm.11227> and using VAD mode at <https://www.fdr.uni-hamburg.de/record/11394>. The microwave radiometer observations can be found at <https://doi.org/10.25592/uhhfdm.10198>, the radiosondes profiles can be found at <https://www.fdr.uni-hamburg.de/record/10279> and the data from the network observations by APOLLO and WXT weather stations can be found at <https://www.fdr.uni-hamburg.de/record/10179>.

## Acknowledgments

This work was carried out in the framework of the Hans-Ertel-Centre for Weather Research. We thank the instrument operators for carrying out the measurements during FESSTVaL, as well as the German Weather Service and Julian Steinheuer for providing the Doppler wind lidar data. This research was supported by the Hans-Ertel-Centre for Weather Research, “Climate Monitoring and Diagnostic” phase III (grant no. BMVI/DWD 4818DWD5A).

## References

- Andreas, E. L., Claffy, K. J., & Makshtas, A. P. (2000, dec). Low-Level Atmospheric Jets And Inversions Over The Western Weddell Sea. *Boundary-Layer Meteorology*, 97(3), 459–486. Retrieved from <http://link.springer.com/10.1023/A:1002793831076> doi: 10.1023/A:1002793831076
- Angevine, W. M., Tjernström, M., & Žagar, M. (2006). Modeling of the coastal boundary layer and pollutant transport in new england. *Journal of applied meteorology and climatology*, 45(1), 137–154.
- Banta, R., Newsom, R. K., Lundquist, J. K., Pichugina, Y. L., Coulter, R. L., & Mahrt, L. (2002, nov). Nocturnal Low-Level Jet Characteristics Over Kansas During Cases-99. *Boundary-Layer Meteorology*, 105(2), 221–252. Retrieved from <http://link.springer.com/10.1023/A:1019992330866> doi: 10.1023/A:1019992330866
- Beyrich, F. (1994). Sodar observations of the stable boundary layer height in relation to the nocturnal low-level jet. *Meteorologische Zeitschrift. Neue Folge (Berlin)*, 3(1), 29–34.
- Blackadar, A. K. (1957, may). Boundary Layer Wind Maxima and Their Significance for the Growth of Nocturnal Inversions. *Bulletin of the American Meteorological Society*, 38(5), 283–290. Retrieved from <https://journals.ametsoc.org/doi/10.1175/1520-0477-38.5.283> doi: 10.1175/1520-0477-38.5.283
- Bony, S., Stevens, B., Frierson, D. M., Jakob, C., Kageyama, M., Pincus, R., ... others (2015). Clouds, circulation and climate sensitivity. *Nature Geoscience*, 8(4), 261–268.
- Borque, P., Nesbitt, S. W., Trapp, R. J., Lasher-Trapp, S., & Oue, M. (2020). Observational study of the thermodynamics and morphological characteristics of

- a midlatitude continental cold pool event. *Monthly Weather Review*, 148(2), 719–737.
- Chen, R., & Tomassini, L. (2015). The role of moisture in summertime low-level jet formation and associated rainfall over the east asian monsoon region. *Journal of the Atmospheric Sciences*, 72(10), 3871–3890.
- de Szoeko, S. P., Skillingstad, E. D., Zuidema, P., & Chandra, A. S. (2017). Cold pools and their influence on the tropical marine boundary layer. *Journal of the Atmospheric Sciences*, 74(4), 1149–1168.
- Emeis, S. (2014). Wind speed and shear associated with low-level jets over northern germany. *Meteorol. Z*, 23(3), 295.
- Feng, Z., Hagos, S., Rowe, A. K., Burleyson, C. D., Martini, M. N., & de Szoeko, S. P. (2015). Mechanisms of convective cloud organization by cold pools over tropical warm ocean during the amie/dynamo field campaign. *Journal of Advances in Modeling Earth Systems*, 7(2), 357–381.
- Goff, R. C. (1976). Vertical structure of thunderstorm outflows. *Monthly Weather Review*, 104(11), 1429–1440.
- Gutierrez, W., Araya, G., Kiliyanpilakkil, P., Ruiz-Columbie, A., Tutkun, M., & Castillo, L. (2016, mar). Structural impact assessment of low level jets over wind turbines. *Journal of Renewable and Sustainable Energy*, 8(2), 023308. Retrieved from <http://aip.scitation.org/doi/10.1063/1.4945359> doi: 10.1063/1.4945359
- Hallgren, C., Arnqvist, J., Ivanell, S., Körnich, H., Vakkari, V., & Sahlée, E. (2020). Looking for an offshore low-level jet champion among recent reanalyses: a tight race over the baltic sea. *Energies*, 13(14), 3670.
- Han, Y., Yang, Q., Liu, N., Zhang, K., Qing, C., Li, X., ... Luo, T. (2021). Analysis of wind-speed profiles and optical turbulence above gaomeigu and the tibetan plateau using era5 data. *Monthly Notices of the Royal Astronomical Society*, 501(4), 4692–4702.
- Heinold, B., Knippertz, P., Marsham, J., Fiedler, S., Dixon, N., Schepanski, K., ... Tegen, I. (2013). The role of deep convection and nocturnal low-level jets for dust emission in summertime west africa: Estimates from convection-permitting simulations. *Journal of Geophysical Research: Atmospheres*, 118(10), 4385–4400.
- Hohenegger, C., Ament, F., Beyrich, F., Löhnert, U., Rust, H., Bange, J., ... Wolz, K. (in review). Fesstval: the field experiment on submesoscale spatio-temporal variability in lindenbergl. *Bulletin of the American Meteorological Society*.
- Kalverla, P. C., Duncan, J. B., Steeneveld, G. J., & Holtslag, A. A. (2019). Low-level jets over the north sea based on ERA5 and observations: Together they do better. *Wind Energy Science*, 4(2), 193–209. doi: 10.5194/wes-4-193-2019
- Kalverla, P. C., Duncan Jr, J. B., Steeneveld, G.-J., & Holtslag, A. A. (2019). Low-level jets over the north sea based on era5 and observations: together they do better. *Wind Energy Science*, 4(2), 193–209.
- Kirsch, B. (2022). *Illuminating convective cold pools with a dense station network* (Unpublished doctoral dissertation). Max-Planck-Institut für Meteorologie, The International Max Planck Research School on Earth System Modelling, Bundesstrasse 53, 20146 Hamburg.
- Kirsch, B., Ament, F., & Hohenegger, C. (2021). Convective cold pools in long-term boundary layer mast observations. *Monthly Weather Review*, 149(3), 811–820.
- Kirsch, B., Hohenegger, C., Klocke, D., & Ament, F. (2022). *Meteorological network observations by apollo and wxt weather stations during fesstval 2021*. Universität Hamburg. Retrieved from <https://www.fdr.uni-hamburg.de/record/10179> doi: 10.25592/uhhfdm.10179
- Kirsch, B., Hohenegger, C., Klocke, D., Senke, R., Offermann, M., & Ament, F. (2022). Sub-mesoscale observations of convective cold pools with a dense station network in hamburg, germany. *Earth System Science Data*, 14(8),

- 3531–3548.
- Kirsch, B., Stiehle, B., Löhnert, U., & Ament, F. (2022). *Radiosonde profile measurements during fesstval 2021*. Universität Hamburg. Retrieved from <https://www.fdr.uni-hamburg.de/record/10279> doi: 10.25592/uhhfdm.10279
- Lampert, A., Bernalte Jimenez, B., Gross, G., Wulff, D., & Kenull, T. (2016, oct). One-year observations of the wind distribution and low-level jet occurrence at Braunschweig, North German Plain. *Wind Energy*, 19(10), 1807–1817. Retrieved from <http://doi.wiley.com/10.1002/we.1951> doi: 10.1002/we.1951
- Luiz, E. W., & Fiedler, S. (2022). Spatiotemporal observations of nocturnal low-level jets and impacts on wind power production. *Wind Energy Science*, 7(4), 1575–1591.
- Löhnert, U., Knist, C., Böck, T., & Pospichal, B. (2022). *Microwave radiometer observations during fesstval 2021*. Universität Hamburg. Retrieved from <https://www.fdr.uni-hamburg.de/record/10198> doi: 10.25592/uhhfdm.10198
- Mahrt, L., Vickers, D., & Andreas, E. L. (2014). Low-level wind maxima and structure of the stably stratified boundary layer in the coastal zone. *Journal of Applied Meteorology and Climatology*, 53(2), 363–376.
- Mueller, C. K., & Carbone, R. E. (1987). Dynamics of a thunderstorm outflow. *Journal of the Atmospheric sciences*, 44(15), 1879–1898.
- Päschke, E., Leinweber, R., & Lehmann, V. (2015). An assessment of the performance of a 1.5  $\mu\text{m}$  Doppler lidar for operational vertical wind profiling based on a 1-year trial. *Atmospheric Measurement Techniques*, 8(6), 2251–2266. doi: 10.5194/amt-8-2251-2015
- Schepanski, K., Tegen, I., Todd, M. C., Heinold, B., Bönisch, G., Laurent, B., & Macke, A. (2009). Meteorological processes forcing saharan dust emission inferred from msg-seviri observations of subdaily dust source activation and numerical models. *Journal of Geophysical Research: Atmospheres*, 114(D10). doi: <https://doi.org/10.1029/2008JD010325>
- Shapiro, A., & Fedorovich, E. (2010, jul). Analytical description of a nocturnal low-level jet. *Quarterly Journal of the Royal Meteorological Society*, 136(650), 1255–1262. Retrieved from <http://doi.wiley.com/10.1002/qj.628> doi: 10.1002/qj.628
- Sisterson, D. L., & Frenzen, P. (1978, feb). Nocturnal boundary-layer wind maxima and the problem of wind power assessment. *Environmental Science & Technology*, 12(2), 218–221. Retrieved from <https://pubs.acs.org/doi/abs/10.1021/es60138a014> doi: 10.1021/es60138a014
- Steinheuer, J., Detring, C., Beyrich, F., Löhnert, U., Friederichs, P., & Fiedler, S. (2022). A new scanning scheme and flexible retrieval for mean winds and gusts from doppler lidar measurements. *Atmospheric Measurement Techniques*, 15(10), 3243–3260.
- Svensson, N., Bergström, H., Rutgersson, A., & Sahlée, E. (2019, jun). Modification of the Baltic Sea wind field by land-sea interaction. *Wind Energy*, 22(6), 764–779. Retrieved from <https://onlinelibrary.wiley.com/doi/abs/10.1002/we.2320> doi: 10.1002/we.2320
- Terai, C., & Wood, R. (2013). Aircraft observations of cold pools under marine stratocumulus. *Atmospheric Chemistry and Physics*, 13(19), 9899–9914.
- Tuononen, M., O’Connor, E. J., Sinclair, V. A., & Vakkari, V. (2017). Low-level jets over Utö, Finland, based on Doppler lidar observations. *Journal of Applied Meteorology and Climatology*, 56(9), 2577–2594.
- Udina, M., Soler, M., Viana, S., & Yagüe, C. (2013). Model simulation of gravity waves triggered by a density current. *Quarterly Journal of the Royal Meteorological Society*, 139(672), 701–714.

- 487 Van de Wiel, B. J. H., Moene, A. F., Steeneveld, G. J., Baas, P., Bosveld, F. C., &  
 488 Holtslag, A. A. M. (2010, aug). A Conceptual View on Inertial Oscillations  
 489 and Nocturnal Low-Level Jets. *Journal of the Atmospheric Sciences*, 67(8),  
 490 2679–2689. Retrieved from [https://journals.ametsoc.org/doi/10.1175/](https://journals.ametsoc.org/doi/10.1175/2010JAS3289.1)  
 491 2010JAS3289.1 doi: 10.1175/2010JAS3289.1
- 492 Wagner, D., Steinfeld, G., Witha, B., Wurps, H., & Reuder, J. (2019). Low level jets  
 493 over the southern North Sea. *Meteorologische Zeitschrift*, 28(5), 389–415. doi:  
 494 10.1127/metz/2019/0948
- 495 Ziemann, A., Galvez Arboleda, A., & Lampert, A. (2020). Comparison of Wind  
 496 Lidar Data and Numerical Simulations of the Low-Level Jet at a Grassland  
 497 Site. *Energies*, 13(23), 6264. doi: 10.3390/en13236264